Collapse of a cohesive granular column

A. Gans, A. Abramian, Pierre-Yves Lagrée, M. Gong, A. Sauret, O. Pouliquen, M. Nicolas

Collapse of a cohesive granular column

A. Gans[1], A. Abramian[2], P.-Y. Lagrée[2], M. Gong[3], A. Sauret[3], O. Pouliquen[1], and M.Nicolas[1] †

[1]Aix Marseille Univ, CNRS, IUSTI, Marseille, France

[2]Sorbonne Université, CNRS, Institut Jean le Rond d'Alembert, Paris, France

[3]Department of Mechanical Engineering University of California, Santa Barbara, USA

(Received xx; revised xx; accepted xx)

The collapse of a column of cohesive granular media is investigated both experimentally and numerically in the framework of a continuum model. The configuration is an initial parallelipipedic granular pile, which is suddenly released by opening a retaining door. In experiments, we use a model material developed by (Gans et al. 2020) made of silica particles coated with poly-boro-siloxane, for which the adhesive inter particle force can be tuned by controlling the thickness of the coating. Numerically, the collapse is simulated using a simple cohesive rheological model implemented in a 2D Navier-Stokes-solver. We investigate the role of the cohesion on the stability of the column, on the mode of failure, on the flow dynamics and on the geometry of the final deposit, showing that the continuum model predicts the main features observed experimentally.

Key words:

1. Introduction

Cohesive granular materials are encountered in many geophysical and industrial applications. Whereas many advances have been made in the description of cohesionless granular flows in various configurations, the behavior of cohesive granular media has been much less investigated. One difficulty is the complexity underlying the origin of cohesion. For very small particles (typically below 10 μm in diameter), the cohesion arises from attractive forces like Van der Walls (Castellanos 2005) or electrostatic forces (Konopka & Kosek 2017), whereas for larger particles it may arise from capillary bridges (Bocquet et al. 1998; Mitarai & Nori 2006) or from solid bridges (Langlois et al. 2015). In materials encountered in applications, adhesive force between grains may also evolve due to the variation of the environmental conditions (change of the confinement pressure, of the temperature, of the humidity rate) or due to the micro-mechanical evolution of the bonds (ageing, sintering, chemical reaction). This complexity in controlling cohesion explains why most of the fundamental experimental studies focus on humid granular materials, for which the cohesion is controlled by the amount of liquid mixed to the grains. Flows in rotating drums, granular collapse have been

† Email address for correspondence: maxime.nicolas@univ-amu.fr

investigated using unsaturated granular media. However, capillary bridges are known to migrate, to merge during flow, which adds some heterogeneities and complexity in the flow. Recently another model granular material has been developed (Gans et al. 2020), where the cohesion originates from a polyborosilicate (PBS) coating of the glass particles. The resulting cohesive material is very stable, is reusable, and the adhesive force is constant in time simply controlled by the thickness of the coating. In this paper, we study the dynamics of this cohesion controlled granular material in the classical configuration of the granular collapse.

The granular collapse, which consists in the sudden release of a granular pile under gravity (Balmforth 2005; Lajeunesse et al. 2005; Lube et al. 2005), has been extensively studied for cohesionless granular materials and has served as a benchmark for both discrete (Lacaze et al. 2008; Kermani et al. 2015) and continuum simulations (L. Staron & Hinch 2005; Lagrée et al. 2011). When the grains are released, the granular mass spreads and stops at a finite distance (Lajeunesse et al. 2005). It has been shown that the morphology of the deposit is mainly controlled by the initial aspect ratio of the column and scaling laws have been evidenced for the runout distance and the final height, which are independent of the material properties. Some studies have investigated the influence of cohesion on the dynamics of the granular collapse. Experimentally, Meriaud and Triantafilliou (Mériaux & Triantafillou 2008) have studied the collapse of fine powders and shows that the cohesion does not modify the scaling laws of the runout but modifies the prefactors. Artoni et al (Artoni et al. 2013) and more recently Li et al (Li et al. 2021) have studied the collapse of wet granular media and how the dynamics depends on both the particle diameters via the Bond number and the water content. Using discrete element method and an irreversible adhesive force model between particles to mimic solid bridges, Langlois et al (Langlois et al. 2015) have shown how fragmentation occurs during the collapse and how it decreases the runout distance. Abramian et al have analysed the stability criterion (Abramian et al. 2020) and the roughness of the free surface (Abramian et al. 2021) of the final deposit, which increases when increasing the adhesive forces between the grains. In this paper we revisit the problem of the collapse of a cohesive granular media, by performing experiments using the new cohesion controlled material, and by confronting the measurement to prediction from continuum simulations using a simple rheological description obtained by adding a constant cohesive stress to the $\mu(I)$ rheology. Although the rheology of cohesive material is known to be more complex (Badetti et al. 2018; Mandal et al. 2021; Macaulay & Rognon 2021), this approach is a first attempt to capture cohesive effects in a continuum model. After the description of the experimental procedure and of the numerical methods in section 2, we focus on the stability condition (section 3) and failure mode of the pile (section 4) and confront the observation to the prediction of a Mohr Coulomb model. The role of the cohesion on the dynamics of the flow, on the typical velocities, and on the shape of the final deposit are discussed in section 5, before concluding in section 6.

2. Experimental and numerical methods

2.1. *Experimental setup and methods*

In our experiments, the controlled-cohesion granular material (CCGM) is made of glass beads of diameter $d = 800 \pm 60$ μm coated with a PolyBoroSilicate (PBS) polymer. To vary the cohesion, we vary the averaged thickness b of the coating in the range $0 < b < 400$ nm. From equation 7 in (Gans et al. 2020), this corresponds to a static cohesive stress τ_c in the range $0 < \tau_c < 65$ Pa. In the following, the cohesion is characterized through the cohesion

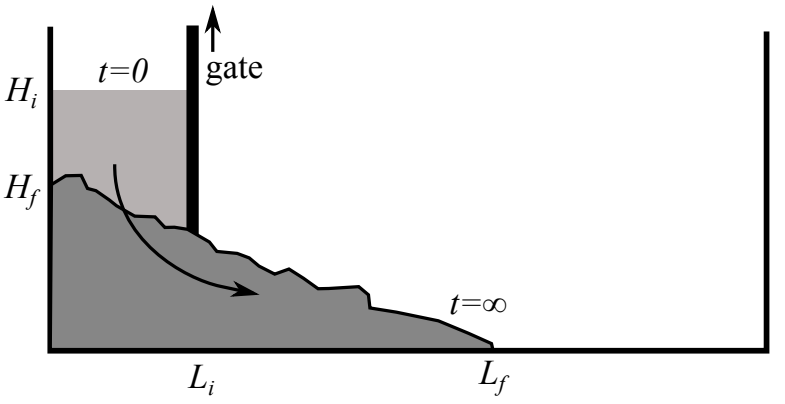

Figure 1: Sketch of the experimental setup showing the initial granular column of length L_i and height H_i (light gray) and the final deposit of length L_f and height H_f (dark gray).

length ℓ_c defined as

$$\ell_c = \frac{\tau_c}{\phi \rho g}, \tag{2.1}$$

which corresponds to the characteristic length for which the hydrostatic pressure $P = \phi \rho g \ell_c$ is equal to the cohesive stress τ_c. In this paper, the particle density is ρ =??, the voume fraction is $\phi \approx$?? and g is the acceleration of the gravity. The range of cohesive lengths investigated in this study is $0 \leqslant \ell_c \leqslant 4.1$ mm.

A sketch of the experimental setup is shown in Fig. 1. It consists of a rectangular channel of length 62 cm, width 15.4 cm and height 31 cm. A mass M of cohesive grains is retained on the left side of the box by a removable gate, which can slide upwards. The rectangular channel is built with PMMA plates and the bottom plate is made rough by gluing particles of the same size as the flowing particles. Since the PBS-coated particles have a very low friction coefficient with PMMA, there is no significant lift nor tangential stress observed neither when opening the gate, nor on the side walls. Different initial columns are used with a length L_i in the range $2.54 < L_i < 12.7$ cm and a height H_i in the range $1 < H_i < 23$ cm. The aspect ratio $a = H_i/L_i$ varies in the range $0.7 < a < 6.6$. At time $t = 0$ the gate is rapidly removed vertically, and the granular mass spreads until it reaches a new static configuration at long time. The final deposit is characterized by its length L_f and its height H_f. The granular collapse is recorded with a high-speed camera (Phantom VEO 710) at 300 fps. A vertical laser sheet illuminates the vertical central plane of the channel, providing a measurement of the pile profile during the flow. Using an image processing software, the spatio-temporal evolution of the profile is computed and the front velocity V and the final deposit geometry are measured.

2.2. *Numerical methods*

In parallel to the experiments, we performed numerical simulations based on the 2D Navier-Stokes solver Basilisk, an open-source library (www.basilisk.fr) using an adaptive mesh and a volume-of-fluid method. The granular material is considered as an incompressible fluid, with a non-newtonian frictional rheology. Without cohesion, it has been shown that the collapse is captured by the simple $\mu(I)$ constitutive law (Lagrée et al. 2011). The stress tensor is given by $\sigma_{ij} = -P\delta_{ij} + \tau_{ij}$, where P is the pressure, and τ_{ij} the deviatoric stress

given by

$$\tau_{ij} = \mu(I) P \frac{\dot{\gamma}_{ij}}{|\dot{\gamma}|} \tag{2.2}$$

where $\dot{\gamma}_{ij}$ is the shear rate tensor, $|\dot{\gamma}| = \sqrt{1/2 \dot{\gamma}_{ij} \dot{\gamma}_{ij}}$ its second invariant, and the friction coefficient μ is a function of the dimensionless inertial number I

$$\mu(I) = \mu_s + \frac{\Delta\mu}{I_0/I + 1}, \quad \text{where} \quad I = \frac{|\dot{\gamma}| d}{\sqrt{P/\rho}}. \tag{2.3}$$

In this study where the cohesion plays an important role, we extend this rheological model by adding a constant cohesive stress τ_c so that the deviatoric stress τ_{ij} becomes (see Abramian et al. (2020) for numerical details)

$$\tau_{ij} = (\tau_c + \mu(I) P) \frac{\dot{\gamma}_{ij}}{|\dot{\gamma}|}. \tag{2.4}$$

In the following, when comparing simulation with the experiments, the value of τ_c in the numerical code is equal to its experimental value, and the parameters of the friction law $\mu(I)$, when not specified, are chosen from a calibration based on the cohesionless case: $\mu_s = 0.4$, $\Delta\mu = 0.12$, and $I_0 = 0.3$. The influence of these numerical parameters are discussed in appendix A. It should be emphasized that in the numerical method the plastic criterion and the existence of a yield stress is not strictly captured. A regularization method is used where a cut-off of the viscosity to a finite but high value is introduced for low values of shear rate (Abramian et al. 2020).

2.3. *Control parameters*

The dynamics of the cohesive granular collapse is *a priori* controlled by three dimensionless numbers: the aspect ratio of the initial column $a = H_i/L_i$, the relative magnitude of the cohesion stress compared to the gravity stress given by the ratio of the cohesive length to the height of the columns ℓ_c/H_i, and the number of particles in the column H_i/d. However, in the limit of a continuum media and in a regime where non local effects are expected to be negligible, which is the main assumption in our continuum simulations, this last number is expected to play no role (the role of the particle diameter on the cohesion being encoded in the cohesion length). The system is thus controlled by only two parameters $a = H_i/L_i$ and ℓ_c/H_i, which are chosen to be equal in the simulation and in the experiments when confronting the experimental observation to the numerical prediction.

2.4. *Qualitative observations*

When the gate of the experimental setup is removed, three different behaviors are observed, depending on the aspect ratio of the column and on the cohesion of the material. When the column is not high enough, it remains static, showing that a minimal height of cohesive material is required to trigger the flow (Fig. 2a). For a slightly higher column, the material breaks along a well defined failure plane having its origin at the foot of the pile, leading to the collapse of the top right corner of the column (Fig. 2b), the rest of the pile remaining undeformed. For a sufficiently high column and/or for a sufficiently weak cohesive force between particles, the collapse starts at the right corner but extends to the bulk leading to the spreading of the granular mass until a new static configuration is reached (Fig. 2c). The final deposit surface reveals a roughness reminiscent of undeformed clusters during the flows Langlois et al. (2015), which increases when increasing the cohesion (Abramian et al. 2020). In particular, the upper right corner of the initial column seems to be carried by the flow

without being sheared or deformed and is present in the final deposit (Fig. 2c).The same phenomenology is observed in simulations as shown in Fig. 2.

3. Column stability

To interpret the initiation of the flow and the failures observed both in experiments and simulations, we express the stability condition of a granular column in the framework of a simple cohesive Mohr-Coulomb model.

3.1. *Theoretical failure conditions*

The failure of hills has been the subject of many studies in the soil mechanics literature (Fredlund & Krahn 1977; Chen et al. 2003; Duncan et al. 2014). Here, we restrict our analysis to the simple assumption that the failure occurs along a straight plane, following the work of Restagno et al. (2004). Three different configurations depicted in Fig. 3 are analyzed: an infinitely wide rectangular pile, a truncated wide pile, and a pile of finite width.

We first consider a cohesive rectangular column of height H_i and width $L_i \gg H_i$. A corner delimited by the slip plane having its origin at the bottom right base and inclined at an angle α from horizontal (Fig. 3a) is stable according to a cohesive Mohr-Coulomb criterion if the following condition is true:

$$Mg \sin\alpha \leqslant S\tau_c + \mu_s Mg \cos\alpha, \tag{3.1}$$

where M is the mass of material above the slip plane, S is the area of the failure surface, μ_s is the static friction angle and τ_c is the cohesive stress. In the configuration of Fig. 3a, $M = \rho W {H_i}^2/2\tan\alpha$ and $S = WH_i/\sin\alpha$, where W is the thickness of the pile. The pile is then stable when

$$\frac{\rho g H_i}{2\tan\alpha}\sin\alpha\,(\sin\alpha - \mu_s\cos\alpha) \leqslant \tau_c \tag{3.2}$$

which can be expressed using the cohesive length ℓ_c and the friction angle $\theta_c = \arctan(\mu_s)$

$$f_{\theta_c}(\alpha) = \frac{\cos\alpha\sin(\alpha-\theta_c)}{2\cos\theta_c} \leqslant \frac{\ell_c}{H_i}. \tag{3.3}$$

The function $f_{\theta_c}(\alpha)$ is drawn in Fig. 3a for $\mu_s = 0.4$ corresponding to $\theta_c = 21.8^o$. This function is a symmetric curve centered at $\alpha_m = \theta_c/2 + \pi/4$, where it reaches its maximum value $f_{\theta_c}(\alpha_m) \approx 0.17$, and becomes zero for $\alpha = \theta_c$ and $\alpha = \pi/2$. In this plot, a point $(\alpha, \ell_c/H_i)$ below the curve corresponds to an unstable corner. A high cohesion level $\ell_c/H_i > 0.17$ corresponds to a stable pile (blue line) for which the stability criterion 3.3 is fulfilled whatever the slip angle α. The value $\ell_c/H_i = 0.17$ corresponds to the marginally stable pile, which will break along the slip plane inclined at α_m (red line). A low cohesion level $\ell_c/H_i < 0.17$ corresponds to an unstable column that may fail at any angle for which $f_{\theta_c}(\alpha) > \ell_c/H_i$ (green line).

This analysis can be generalized to the case of a truncated pile, with a missing corner inclined at an angle θ_m (Fig. 3b). Studying this geometry is interesting as it may provide information about the stable final deposit shape. By evaluating the mass of material M located between the slip plane inclined at an angle α and the free surface inclined at an angle θ_m, one can derive the following expression for the stability criterion:

$$\frac{1}{2}\rho g H_i\left(\frac{1}{\tan\alpha} - \frac{1}{\tan\theta_m}\right)(\sin\alpha - \mu\cos\alpha) \leqslant \tau_c. \tag{3.4}$$

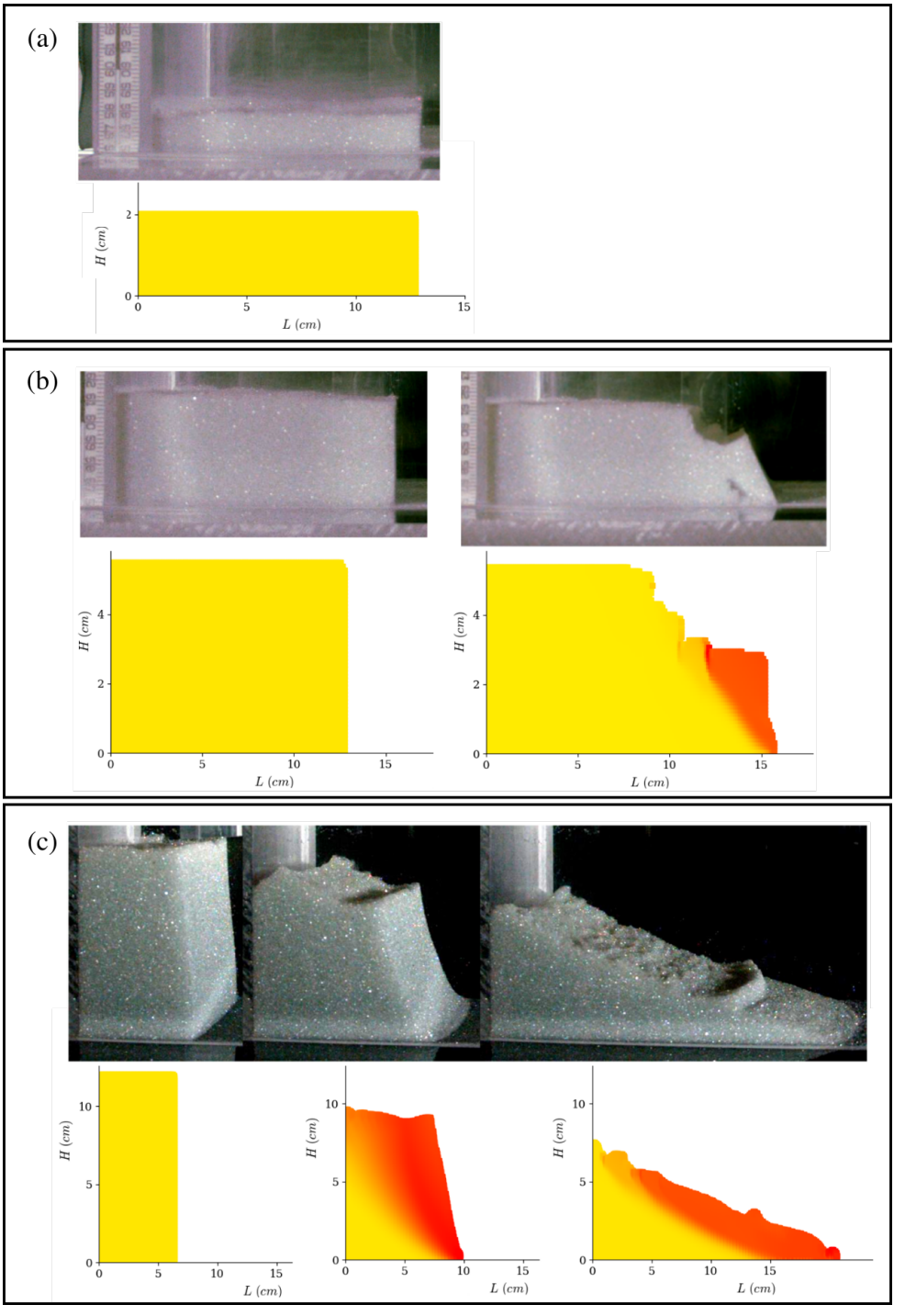

Figure 2: Experimental observations (top gray pictures) and numerical simulation (bottom color pictures) of the collapse of a cohesive granular column.(a) A stable column with small aspect ratio ($a = 0.08$, $\ell_c = 4.1$ mm)(b) Partial collapse for a moderate aspect ratio ($a = 0.43$, $\ell_c = 4.1$mm) with a well defined slip plane. (c) Collapse of the column ($a = 1.9$, $\ell_c = 2.8$mm), where we observe a 'surfing wedge' coming from the top right corner being transported during the flow.

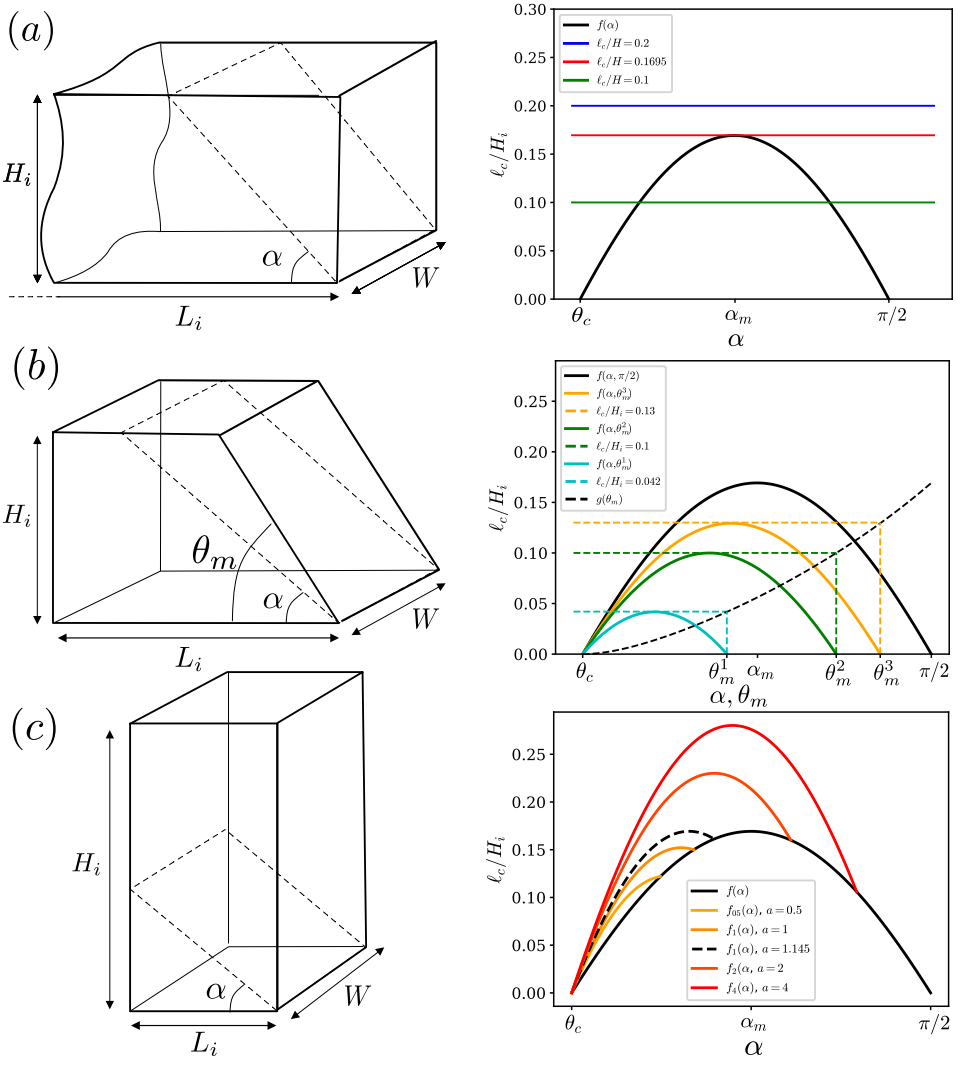

Figure 3: Theoretical analysis of the stability of columns using a cohesive Mohr-Coulomb criterion. (a) a wide column: the corner delimited by the plane inclined at an angle α is stable when the cohesion level ℓ_c/H_i is above the black curve $f_{\theta_c}(\alpha)$ (eq. 3.3). The blue line correspond to a cohesion level leading to stable column, the red line to marginally stable column where a single angle $\alpha_m = \theta_c/2 + \pi/4$ is unstable, the green line corresponds to an unstable column. (b) a truncated pile: the different curves corresponds to the stability function $f_{\theta_c,\theta_m}(\alpha)$ (eq. 3.5) for different values of the free surface inclination θ_m ($\theta_m^1 = ??^o$, $\theta_m^2 = ??^o$, $\theta_m^3 = ??^o$). The dashed line shows how the critical cohesion level above which the pile is stable varies with the angle θ_m. (c) a tall column: the stability curves for different aspect ratio a given by $f_{\theta_c,a}(\alpha)$ (eq. 3.8) for $\alpha < \arctan a$. and by $f_{\theta_c}(\alpha)$ (eq. 3.3) for $\alpha > \arctan a$.

Using again ℓ_c and θ_c, this equation may be rewritten as :

$$f_{\theta_c,\theta_m}(\alpha) = \frac{\sin(\theta_m - \alpha)\sin(\alpha - \theta_c)}{2\cos\theta_c \sin\theta_m} \leqslant \frac{\ell_c}{H_i} \tag{3.5}$$

The different stability limits in the plane $\alpha, \ell_c/H_i$ for different truncated angles θ_m are plotted in Fig. 3b. The graphs of the function $f_{\theta_c,\theta_m}(\alpha)$ are curves centered in $(\theta_c + \theta_m)/2$ and vanishing at $\alpha = \theta_c$ and $\alpha = \theta_m$. The rectangular pile is recovered for $\theta_m = \pi/2$. The maximum of the $f_{\theta_c,\theta_m}(\alpha)$ gives the value of the critical cohesion level $(\ell_c/H_i)_{crit}(\theta_m)$ below which the pile truncated at angle θ_m is unstable, given by the following equation:

$$(\ell_c/H_i)_{crit} = \frac{1 - \cos(\theta_m - \theta_c)}{4\cos\theta_c \sin\theta_m} = \frac{\ell_c}{H_i} \tag{3.6}$$

This function $(\ell_c/H_i)_{crit}(\theta_m)$ is plotted in Fig. 3b as dashed line. A pile truncated at an angle θ_m and for a cohesion level ℓ_c/H_i such that the point $(\theta_m, \ell_c/H_i)$ is below this line is unstable.

The last case of interest is the case when the aspect ratio of the pile is large and that the slip plane no longer intersects the top free surface but the left side of the pile, *i.e.* when $\arctan a \geqslant \alpha$ (Fig. 3c). In this case, $M = \rho W L_i(H_i - \frac{1}{2}L_i\tan\alpha)$ and $S = WL_i/\cos\alpha$, and the stability criterion of the column is given by:

$$\rho g\left(H_i - \frac{L_i\tan\alpha}{2}\right)\cos\alpha\,(\sin\alpha - \mu_s\cos\alpha) \leqslant \tau_c \tag{3.7}$$

that can be written as

$$f_{\theta_c,a}(\alpha) = \left(1 - \frac{1}{a}\frac{\tan\alpha}{2}\right)\cos^2\alpha\,(\tan\alpha - \tan\theta_c) \leqslant \frac{\ell_c}{H_i} \tag{3.8}$$

The stability criterion in this case depends on the aspect ratio a and is given by the function $f_{\theta_c,a}(\alpha)$, which is plotted as curves starting at $(\alpha = \theta_c, 0)$ and presenting a maximum. This maximum increases when increasing the aspect ratio. When the slip angle α reaches the $\arctan a$ value, i.e the slip plane no longer reach the left vertical side of the column, the stability criterion is no longer given by the $f_{\theta_c,a}(\alpha)$ function but by the low aspect ratio function $f_{\theta_c}(\alpha)$ (Eq. 3.3). For a given aspect ratio a, the stability of the column is thus given by a curve made of two parts as shown in Fig. 3c, its absolute maximum giving the critical cohesion level below which the pile is unstable. At low aspect ratio the first part of the curve (color curves in Fig. 4) is lower than the second part (black curve) and the stability is controlled by a constant cohesion level, independent of a. When a becomes greater than 1.145 (Black dashed line in Fig. 3c), the maximum is given by the first maximum corresponding to a mode of failure crossing the pile from one side to another. A stability limit can then be plotted in a $(a, \ell_c/H_i)$ plane, as shown by the black curve in Fig. 4, separating the stable region (blue) from the region where collapse occurs (pink). The discontinuity between the two geometrical possibilities of failure occurs at $a \approx 1.145$.

3.2. *Experimental and numerical observations*

We first investigated experimentally the condition for a collapse of the pile after the opening of the gate. Numerous experiments were done changing both the aspect ratio a and the cohesive strength ℓ_c/H_i. The results are plotted in Fig. 4 as circles with the following color code: red color indicates that a collapse occurs, blue color indicates that the column remains stable. Experimentally, we were not able to investigate the high aspect ratio and large ℓ_c/H_i limit, as for the range of ℓ_c accessible with our beads, it would correspond to very narrow pile with only few particles in the width.

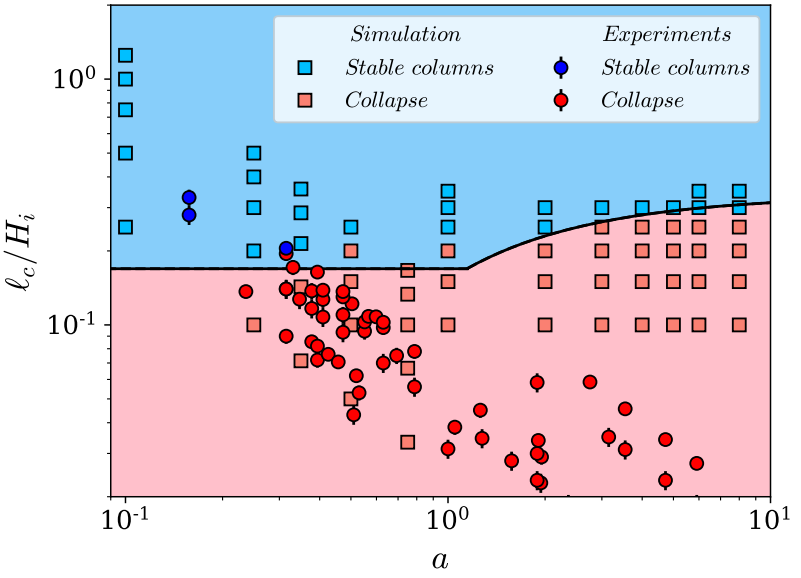

Figure 4: Stability diagram in the plane (aspect ratio a-cohesion level ℓ_c/H_i) for a cohesive granular column. The black curve is the limit of stability. Circles corresponds to experiments, squares to simulation and blue (resp. red) symbols correspond to stable (resp. unstable) columns.

The numerical results are data taken from Abramian et al. (2020) and data from new computations, and the results are plotted as square symbols, with the same color code as before. Both experimental and numerical results show good agreement with the Mohr-Coulomb stability criterion showing that the the limit of stability of a cohesive granular pile is well captured by a simple Mohr-Coulomb model.

4. Collapse angles

The above theoretical stability analysis predicts whether a column of aspect ratio a and cohesion level ℓ_c/H_i between grains is stable or unstable and gives a range of potential failure angles. However, it does not predict which angle is selected. To characterise how the column breaks, we identify two different angles in experiments and numerical simulations. A first angle is the initial angle of failure α_i, which delimits the upper right corner collapsing at the onset of the flow. Experimentally to determine α_i we compare a reference image of the static column with the subsequent images at the onset of the flow using an image subtraction process enhanced with a threshold filter. Numerically, we threshold the velocity field at the initiation of the flow. A second angle is the final angle α_f of the plane below which no grain has moved during the whole flow. This angle is experimentally measured through an image difference process between the initial reference image and the images recorded at the end of the collapse, and numerically by thresholding the integral of the velocity field during the whole dynamics.

The experimental and numerical results are reported in Fig. 5, where we restrict the analysis to the small aspect ratio configuration (Fig. 3a). In the simulations the initial failure angle α_i (red open circles) is constant whatever the parameters and is always close to the critical angle $\alpha_m = \theta_c/2 + \pi/4 \approx 0.55^o$. The final failure angle α_f (red dots) delimiting the pile where grains never move is equal to the initial one α_i for large cohesion levels $\ell_c/H_i \gtrsim 0.08$. This

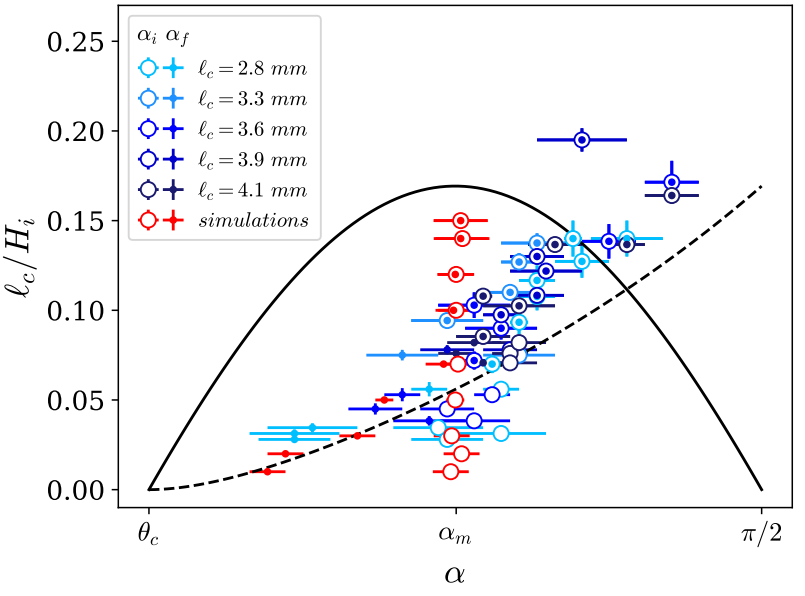

Figure 5: Measurements of the initial failure angle α_i (open circles) and final angle of stability α_f (filled disks) for different cohesion level ℓ_c/H_i. Red symbols are from numerical simulations, blue symbols from experiments. The continuous curve is Eq. 3.3. The dashed line corresponds to Eq.3.6 giving the limity of stability of truncated piles.

means that in in this regime only the first unstable corner flows, the rest of the pile remaining static, as illustrated in Fig 2b. For lower cohesion levels $\ell_c/H_i < 0.08$, the final angle α_f is no longer equal to α_i but decreases and tends to the friction angle for a cohesionless material θ_c when cohesion vanishes. The observation is slightly different in experiments. Contrary to the simulation, the initial failure angle (blue open circles) is not constant whatever the cohesion level. As in the simulation it is close to the critical angle α_m at low cohesion but the experimental α_i increases when increasing the cohesion and becomes larger than what is predicted in the simulation. However, the final angle α_f (blue dots) is equal to α_i for $\ell_c/H_i \gtrsim 0.08$ as observed in simulation, which corresponds to a partial collapse of the column limited to the failure of the right upper corner (Fig. 2b). For low cohesion levels, the final angle measured in experiments is similar to the one predicted in simulations and decreases when decreasing the cohesion. Interestingly, in experiments α_f is close to the critical curve computed theoretically for the stability of truncated piles (eq. 3.6, dashed line in Fig. 5), meaning that the column final shape is close to the marginally stable shape. The discrepancy observed between simulation and experiments for high cohesion level is the sign that the Mohr-Coulomb model might be insufficient to describe our material.

5. Collapse dynamics, run-out length and final deposit

5.1. *Velocity of the front*

Once the gate is removed, the column collapses and a front propagates. The profile of the pile during the collapse can be extracted in experiments from the high-speed movie and the laser sheet projection. A typical run is presented in Fig. 6 showing both the experimental and numerical results for the same parameters for a weakly cohesive material (aspect ratio $a = 1$, $\ell_c/H_i = 0.0314$). Using the same parameters in simulation (cf §2.2), we find a

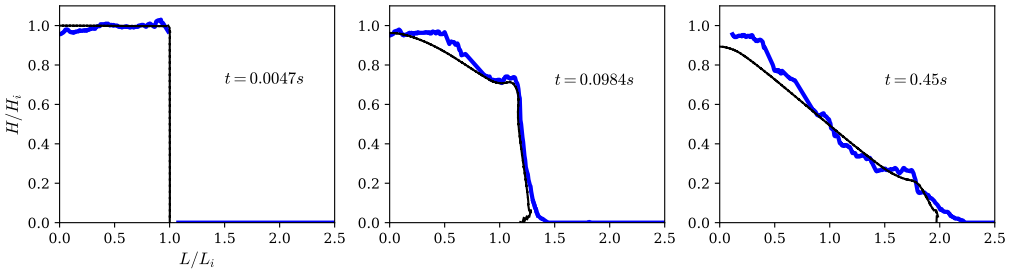

Figure 6: Comparison between the numerical (black) and experimental (blue) profiles of the granular pile at different times for $H_i = 8.9$ cm, $a = 1$, and $\ell_c = 2.8$ mm.

fairly good agreement between experiments and numerical prediction for the dynamics of the pile profile during the collapse. The dynamics of the front and its position $L(t)$ can be determined by measuring the location $L(t)$ of the foot of the pile both in experiments and simulations. The experimental results $L(t) - L_i$ are plotted as solid lines in Fig. 7a, for $\ell_c = 0$ (cohesionless material), $\ell_c = 2.8$ mm and $\ell_c = 3.6$ mm, for an aspect ratio $a = 1$. As a comparison, numerical simulations with the same cohesion levels and same aspect ratio are plotted with dashed lines. We observe that after a short acceleration step, the front travels at a constant velocity before decelerating and eventually reaching a static position. The comparison between experimental and numerical results shows a good agreement from the beginning to the end of the steady state. The agreement is very good for the cohesionless granular experiment (light blue curves) showing that the granular collapse is well described by the continuous numerical code with the $\mu(I)$ rheology. However, in the case of cohesive materials, a difference is observed between experiments and simulation when the flow slows down and stops. The final run-out length is systematically shorter in the numerical simulations for cohesive materials compared to the experiments, as can be also observed in Fig. 6.

Another discrepancy is observed at lower aspect ratio ($a = 0.5$), close to the stability limit (inset of Fig. 7a for a smaller aspect ratio and $\ell_c = 3.6mm$), for which the experiments reveal a delay between the opening of the gate and the initiation of the flow. This delay is not observed in the simulation, and may be reminiscent of more complex rheological feature induced by the thick polymer coating, leading to some creeping phenomena not taken into account in the simple rheological model used in the simulation.

Despite this discrepancy, the velocity of the front $V(t)$ is quantitatively predicted by the simulation as shown in Fig. 7b. The velocity $V(t)$ is defined as the velocity at the inflexion point in $L(t) - L_i$ curves of Fig. 7a. The velocity increases with the aspect ratio up to a plateau when $a \approx 3$. The graph also shows that the velocity decreases when the cohesion increases. .

5.2. *Run-out and final deposit*

Once the kinetic energy of the collapse is fully dissipated, we measure the final deposit and focus on the final run-out length $L_f = L_i + \Delta L$. As shown by (Lajeunesse et al. 2005), the run-out length and the final height of a cohesionless granular material scales as a power law of the aspect ratio a:

$$\frac{\Delta L}{L_i} \propto \begin{cases} a & \text{for } a \leqslant 3 \\ a^{2/3} & \text{for } a \geqslant 3 \end{cases} \quad \text{and} \quad \frac{H_f}{L_i} \propto \begin{cases} a & \text{for } a \leqslant 0.7 \\ a^{1/3} & \text{for } a \geqslant 0.7 \end{cases} \tag{5.1}$$

The results for L_f and H_f obtained with cohesionless and cohesive materials are plotted in Fig. 8, where filled symbols are experimental results, and open symbols are numerical

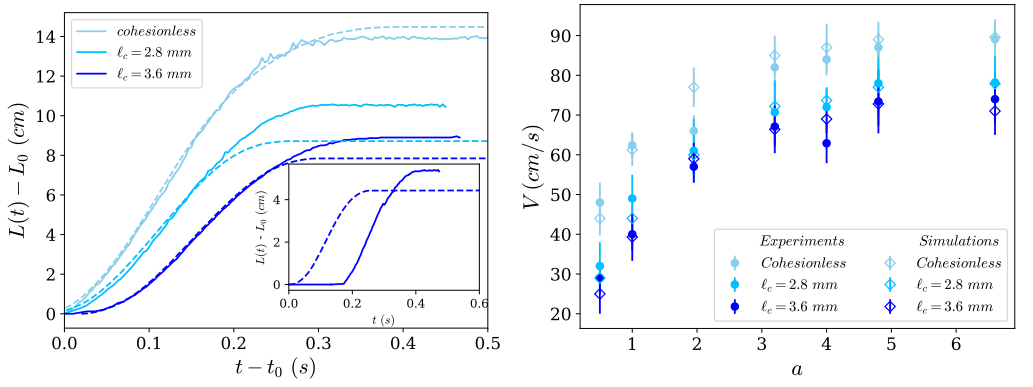

(a) (b)

Figure 7: (a) Time evolution of the front position for different cohesion levels in experiments (continuous curves) and simulations (dashed curves) for an aspect ratio $a = 1$. Inset: results for $a = 0.5$ showing the existence of a significant delay before the collapse occurs for the most cohesive material (dark blue, $\ell_c = 3.6$ mm). (b) Velocity of the front V as a function of the aspect ratio a for different cohesion levels. The color code is the same as in (a).

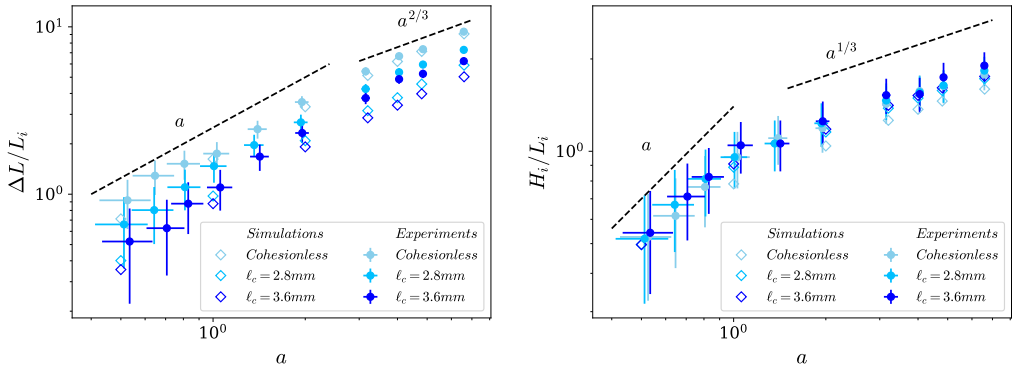

(a) (b)

Figure 8: (*a*) Normalized run-out length $\Delta L/L_i$ as a function of the aspect ratio a for different cohesion levels for both experiments and simulations. (*b*) Normalized height of final deposit H_f/H_i as a function of the aspect ratio a.

results. The run-out length L_f decreases when increasing the cohesion but the final height H_f remains constant. However, the power laws (5.1) are unchanged compared to the cohesionless case, as seen by the a^1 and $a^{2/3}$ slopes on the graph. The cohesion thus only changes the pre-factor on the run-out length (Eqs. 5.1), without changing the exponent of the aspect ratio, as observed with powders by Mériaux & Triantafillou (2008).

As discussed previously, the final run-out predicted by the simulations are not in very good agreement with the experiments for the cohesive materials and systematically underestimate the run-out. Looking more precisely at the morphology of the free surface at the end of the flow reveals that the discrepancy is localized at the tip of the deposit. The no-slip boundary condition applied in the simulation at the contact line may be a source of additional dissipation explaining the difference between simulation and experiments. We show in the appendix that by adjusting the parameters of the rheological model, μ_s, $\Delta\mu$ and I_0 the run-out can be

adjusted, but we found no set of parameters able to predict both cohesionless and cohesive systems.

6. discussion and conclusion

In this paper we studied the dynamics of the collapse of a column of cohesive granular material both experimentally using a controlled cohesive granular materials made of polymer coated particles, and numerically in simulation using a continuous approach based on a cohesive visco-plastic rheology.

The first effect of the cohesion is the stabilization of a granular column with stability criterion depending on the aspect ratio and the cohesion level. The stability criterion and the angle of failure have been measured and compared with a simple theoretical approach based on a Mohr-Coulomb stability criterion assuming a plane of failure.

A second effect of the cohesion is the increase of the dissipation during the flow, leading to a slower spreading of the material and to a shorter run-out length. A striking effect of the cohesion on the collapse of the granular column is the 'surfing wedge' on the top corner of the column. It acts as a dead volume simply transported by the granular flow underneath.

The comparison of the results (stability of the column, run-out length, collapse velocity) between the experiments and the continuous numerical simulation reveals a relatively good agreement, despite some discrepancies. This shows that the main features of the cohesive granular collapse are captured by simply adding a constant cohesive yield stress to the cohesionless granular rheological model. Differences between experiments and simulations were observed for large cohesion levels, for which the initial failure angle is higher in experiments than in simulation, the run-out is underestimated in the simulation, and a delay before the collapse is observed in experiments and not captured in simulations. These differences may come from an oversimplified description of the rheological properties of the cohesive granular material. Additional studies with other configurations more sensitive to rheological details than column collapse would be interesting to further investigate the rheological properties of the material.

This work is part of the COPRINT project and was supported by the ANR grant ANR-17-CE08-0017.

Appendix A. Effect of the rheological parameters

The rheological model implemented in the numerical simulations is set by three arbitrary parameters: the static friction coefficient μ_s, the friction coefficient difference $\Delta\mu$ and the inertial number constant I_0 (see equation 2.3). In this model we assume that the cohesion does not change these parameters, however, since the run-out length and the final morphology is not well captured by the model, a deeper investigation is needed. The effect of the friction coefficients difference $\Delta\mu$ is presented in Fig. 9 (*a*). The distance of the front $L(t)$ is plotted as a function of time for a column of cohesion $\ell_c = 2.8$ mm and an aspect ratio $a = 1$. The green area is obtained by changing the value of $\Delta\mu$ from 0 to 0.2. The figure 9 (*b*) shows the associated final profile for a variation of $\Delta\mu$. We observe that an increase of $\Delta\mu$ leads to a decrease of the run-out length. Consequently, changing the value of $\Delta\mu$ allows to adjust the final run-out of the cohesive collapse with only a small change on the velocity of the collapse.

The effect of I_0 is plotted in Fig. 10 (*a*) and the associated run-out profile is plotted in Fig. 10 (*b*) for the configuration described above, and a chosen $\Delta\mu = 0.1$. We see that changing the value of I_0 barely changes the dynamics and the final profile of the run-out, therefore if the cohesion has an impact on this parameter, we do not expect a major effect.

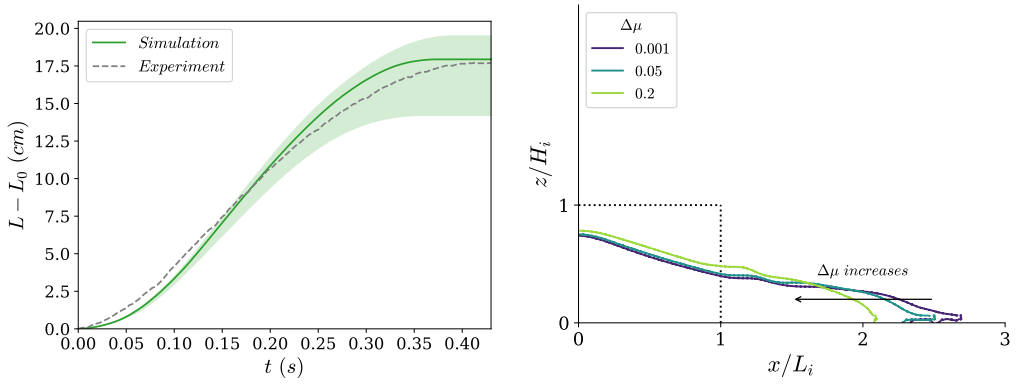

(a) (b)

Figure 9: (*a*) Experimental and numerical front position $L(t)$ of the collapse for $\ell_c = 2.8$ mm, $I_0 = 0.1$ and $a = 1$. The green area is obtained by varying the parameter $\Delta\mu$ from 0 to 0.2, and the green line is the best agreement for the velocity and the run-out. (*b*) Final profiles for 3 values of $\Delta\mu$.

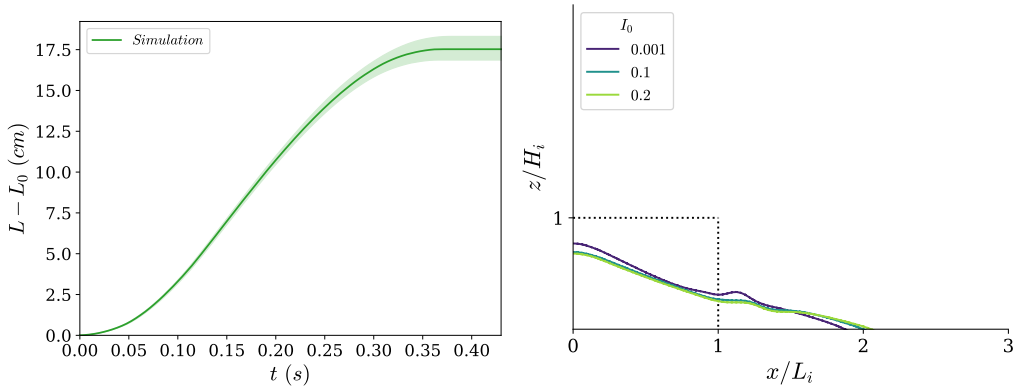

(a) (b)

Figure 10: (*a*) Numerical front position $L(t)$ of the collapse for $\ell_c = 2.8$ mm, $\Delta\mu = 0.1$ and $a = 1$. The green area is obtain by varying the parameter I_0 from 0.001 to 0.2, and the green line is the best agreement for the velocity and the run-out. (*b*) Final profiles for 3 values of I_0.

The last parameter we investigate is the static friction coefficient μ_s. While this parameter has been measured experimentally in a previous study, using inclined plane experiments (Gans et al. 2020), the measurement method was rather different from this setup. However after the initiation of the flow, one may suggest that the PBS coating could act like a lubricant which could decrease the effective μ_s during the flow. An investigation on the effect of the rheological parameter μ_s is presented in Fig. 11. The distance of the front is plotted as a function of the time for an experiment of aspect ratio $a = 1$ and two different simulations with $\mu_s = 0.4$ and $\mu_s = 0.25$. We see that a decrease of μ_s leads to an increase of the velocity and of the run-out length.

With this parametric study, we see that a change of $\Delta\mu$ and μ_s may have a significant impact on the dynamics of the collapse and there might be possible to define an optimal set $(\mu_s, \Delta\mu)$ to fit the experiments. Since in the experiments the PBS coating might change the frictional properties during the flow, we do not know if the apparent effect on μ_s and $\Delta\mu$ is

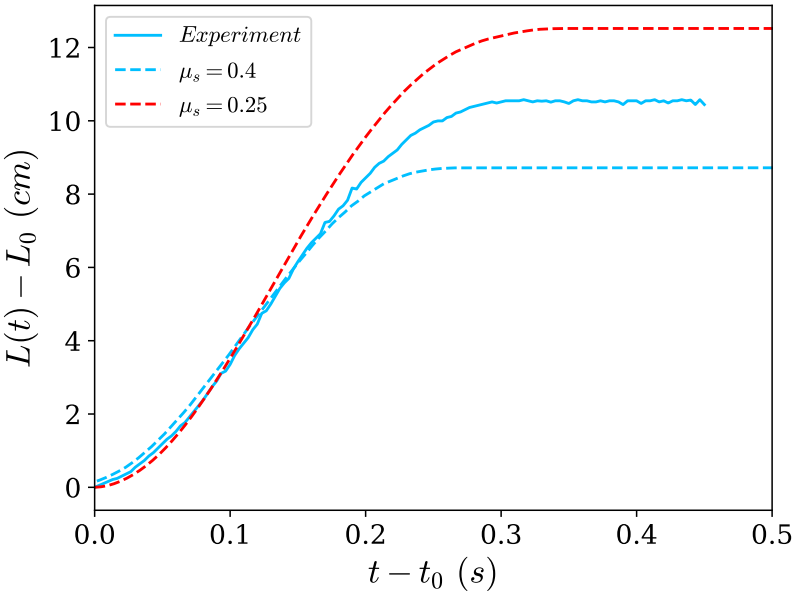

Figure 11: Experimental and numerical front position $L(t)$ of the collapse for $\ell_c = 2.8$ mm, $\Delta\mu = 0.12$, $I_0 = 0.3$ and $a = 1$.

due to cohesion or not. These results suggest that a deeper investigation on the rheology of the CCGM is needed to fully understand its dynamical behavior

REFERENCES

Abramian, Anaïs, Lagrée, Pierre-Yves & Staron, Lydie 2021 How cohesion controls the roughness of a granular deposit. *Soft Matter* **17** (47), 10723–10729.

Abramian, A., Staron, L. & Lagrée, P.-Y. 2020 The slumping of a cohesive granular column: Continuum and discrete modeling. *Journal of Rheology* **64**, 1227–1235.

Artoni, Riccardo, Santomaso, Andrea C, Gabrieli, Fabio, Tono, Diego & Cola, Simonetta 2013 Collapse of quasi-two-dimensional wet granular columns. *Physical Review E* **87** (3), 032205.

Badetti, M, Fall, A, Hautemayou, D, Chevoir, F, Aimedieu, Patrick, Rodts, S & Roux, J-N 2018 Rheology and microstructure of unsaturated wet granular materials: Experiments and simulations. *Journal of rheology* **62** (5), 1175–1186.

Balmforth, N. J. 2005 Granular collapse in two dimensions. *J. Fluid Mech.* **538**, 339–428.

Bocquet, L., Charlaix, E., S., S. Ciliberto & Crassous, J. 1998 Moisture-induced ageing in granular media and the kinetics of capillary condensation. *Nature* **87**, 735–737.

Castellanos, A. 2005 The relationship between attractive interparticle forces and bulk behaviour in dry and uncharged fine powders. *Advances in Physics* **4**, 263–376.

Chen, J., Yin, J.-H. & Lee, C. F. 2003 Upper bound limit analysis of slope stability using rigid finite elements and nonlinear programming. *Canadian Geotechnical Journal* **40**, 742–752.

Duncan, J. M., Wright, S. G. & Brandon, T. L. 2014 Soil strength and slope stability, 2nd edn. Wiley.

Fredlund, D. G. & Krahn, J. 1977 Comparison of slope stability methods of analysis. *Canadian geotechnical journal* **14**, 429–439.

Gans, A., Pouliquen, O. & Nicolas, M. 2020 Cohesion-controlled granular material. *Physical Review E* **101**, 032904.

Kermani, E., Qiu, T. & Li, T. 2015 Simulation of collapse of granular columns using the discrete element method. *Int. J. Geomech* **15**, 04015004.

Konopka, L. & Kosek, J. 2017 Discrete element modeling of electrostatic charging of polyethylene powder particles. *Journal of electrostatics* **87**, 150–157.

L. Staron, L. & Hinch, E. J. 2005 Study of the collapse of granular columns using two-dimensional discrete-grain simulation. *J. Fluid Mech.* **545**, 1–27.

Lacaze, L., Phillips, J.C. & Kerswell, R.R. 2008 Planar collapse of a granular column: Experiments and discrete element simulations. *Physics of fluids* **20**, 063302.

Lagrée, P.Y., Staron, L. & Popinet, S. 2011 The granular column collapse as a continuum: validity of a two-dimensional navier-stokes model with a [mu](i)-rheology. *J. Fluid Mech.* **686**, 378–408.

Lajeunesse, E., Monnier, J. B. & Homsy, G. M. 2005 Granular slumping on a horizontal surface. *Physics of fluids* **17**, 103302.

Langlois, V. J., A., A. Quiquerez & Allemand, P. 2015 Collapse of a two-dimensional brittle granular column: Implications for understanding dynamic rock fragmentation in a landslide. *J. Geophys. Res. Earth Surf.* **120**, 1866–1880.

Li, Pingshan, Wang, Dengming, Wu, Yesheng & Niu, Zhiyang 2021 Experimental study on the collapse of wet granular column in the pendular state. *Powder Technology* **393**, 357–367.

Lube, G., Huppert, H. E., Sparks, R. S. J. & Freundt, A. 2005 Collapses of two-dimensional granular columns. *Physical Review E* **72**, 041301.

Macaulay, Matthew & Rognon, Pierre 2021 Viscosity of cohesive granular flows. *Soft matter* **17** (1), 165–173.

Mandal, Sandip, Nicolas, Maxime & Pouliquen, Olivier 2021 Rheology of cohesive granular media: Shear banding, hysteresis, and nonlocal effects. *Physical Review X* **11** (2), 021017.

Mériaux, C. & Triantafillou, T. 2008 Scaling the final deposits of dry cohesive granular columns after collapse and quasi-static fall. *Phys. Fluids* **20**, 033301.

Mitarai, N. & Nori, F. 2006 Wet granular materials. *Advances in physics* **55**, 1–45.

Restagno, F., Bocquet, L. & Charlaix, E. 2004 Where does a cohesive granular heap break? *European Physical Journal E* **14**, 177–183.